

Variational Quantum Monte Carlo investigations of the superconducting pairing in $\text{La}_3\text{Ni}_2\text{O}_7$

Yi-Qun Liu,¹ Da Wang,^{1,2,*} and Qiang-Hua Wang^{1,2,†}

¹National Laboratory of Solid State Microstructures & School of Physics, Nanjing University, Nanjing 210093, China

²Collaborative Innovation Center of Advanced Microstructures, Nanjing University, Nanjing 210093, China

We investigate the pairing symmetry in the novel superconductor $\text{La}_3\text{Ni}_2\text{O}_7$ under pressure by the non-perturbative variational quantum Monte Carlo. Within the bilayer Hubbard model and extended $t - J$ model with two orbitals in the E_g doublet, we find the local strong correlation triggers s_{\pm} -wave Cooper pairing, with sign change of the gap function among the various Fermi pockets, while the $d_{x^2-y^2}$ -wave pairing is generically disfavored. This is in agreement with the results from functional renormalization group applied in the weak up to moderate correlation limit. We find the $3d_{3z^2-r^2}$ orbital plays a leading role in the superconducting pairing. We also demonstrate the finite intra-orbital double occupancy even in the strong correlation limit, shedding light on the itinerant versus local moment picture of the electrons in this material.

I. INTRODUCTION

The discovery of high-temperature superconductivity in $\text{La}_3\text{Ni}_2\text{O}_7$ ($T_c \approx 80\text{K}$) under pressure [1] triggers extensive research interests both experimentally [2–16] and theoretically [17–60]. The infinite-layer nickelate [61], $\text{R}_3\text{Ni}_2\text{O}_7$ (R is the rare-earth elements) [62, 63], $\text{La}_4\text{Ni}_3\text{O}_{10}$ [64, 65] and other candidates [66] now stand as a new class of high-temperature superconductors besides copper oxide [67]. In this paper, we concentrate on $\text{La}_3\text{Ni}_2\text{O}_7$. It has a bilayer structure, and the orbitals in two layers are hybridized by Ni-O-Ni bonding. This differs from cuprate materials, which are typically monolayer or multi-layer but the coupling between layers are weak [68–70]. In addition to this, both the $3d_{3z^2-r^2}$ (nearly half-filled) and $3d_{x^2-y^2}$ (nearly quarter-filled) orbitals in the E_g -multiplets in $\text{La}_3\text{Ni}_2\text{O}_7$ are active near the Fermi level under high pressure [1, 7, 17, 24] while the cuprate can be treated as a single-orbital system. There are two important questions to ask for the microscopic understanding of superconductivity in $\text{La}_3\text{Ni}_2\text{O}_7$. The first issue is the pairing symmetry. The majority of theories suggest s_{\pm} -wave pairing, with sign change of the gap function among the various Fermi pockets [21–23, 25, 26, 29–31, 35, 37–39], while there are also theories suggesting $d_{x^2-y^2}$ -wave pairing [36, 40, 54, 56] or competition between the two cases of pairing symmetry [28]. The other issue is which orbital plays the dominant role for superconductivity? The viewpoint differs: Either the $3d_{3z^2-r^2}$ orbital dominates [21, 23, 27, 29, 34, 35, 39, 46], or the $3d_{x^2-y^2}$ orbital plays the primary role [25, 26, 37, 45, 49].

$\text{La}_3\text{Ni}_2\text{O}_7$ has been extensively studied within the bilayer two-orbital model by various approaches, such as functional renormalization group (FRG) and renormalized mean field theory (RMFT) [23], random phase approximation (RPA) [31], dynamical mean field theory (DMFT) [56], density matrix renormalization group (DMRG) [51, 55], infinite projected entangled pair states (iPEPS) [49] and slave boson mean field (SBMF) [40, 45], etc. Each approach has its own advantage and limitations. For example, the FRG and RPA work in the itinerant picture, hopefully applicable in the weak

up to moderate correlation regime. The various mean field theories are non-perturbative but suffer from the known problem of ignoring the correlation of fluctuations. The DMFT takes local quantum fluctuations into account but yet the spatial correlations are still inaccessible. The DMRG and iPEPS studies are theoretically exact, but are limited to finite size or finite bond dimension. Moreover, it is not yet clear whether the starting model could be defined in the local moment limit, and even in this limit whether the local moment on the d_{z^2} orbital could be effectively dropped out, assuming the Hund's coupling is also strong. In this work, we use the variational quantum Monte Carlo (VQMC) simulations to study the bilayer Hubbard model and its low energy effective extended $t - J$ model (allowing orbital double occupancy). Within the variational ansatz, the VQMC is able to handle a relatively larger lattice size, and to treat the correlation effects exactly. We compare the optimized ground state energies in the s_{\pm} -wave pairing ansatz and the $d_{x^2-y^2}$ -wave pairing one. We find that, for the Hubbard model, the s_{\pm} -wave pairing symmetry is generically more favorable for not too weak Hund's coupling, and for the extended $t - J$ model, the s_{\pm} -wave pairing always wins. Inspection of the variational pairing amplitudes ascertains that the $3d_{3z^2-r^2}$ orbital predominates in the superconducting pairing. The results are consistent with the conclusion from the FRG study [23]. Moreover, we demonstrate sizable intra-orbital double occupancy in both models up to strong correlation limit, seeding light on the itinerant versus the local moment picture for the electrons in the superconducting $\text{La}_3\text{Ni}_2\text{O}_7$.

The rest of the paper is arranged as follows: We first introduce the two-orbital Hubbard model and its effective $t - J$ model in strong coupling limit in Sec. II. Then, we employ VQMC to study and compare these two models in Sec. III. Finally, a summary is given in Sec. IV.

II. MODEL

To describe the band structure of $\text{La}_3\text{Ni}_2\text{O}_7$, we adopt the two-orbital ($3d_{x^2-y^2}$ and $3d_{3z^2-r^2}$) tight-binding model on a bilayer square lattice given by the following Hamiltonian

$$H_0 = \sum_{i\delta,ab,\sigma} t_{\delta}^{ab} c_{ia\sigma}^{\dagger} c_{i+\delta b\sigma} + \sum_{ia\sigma} \epsilon_a c_{ia\sigma}^{\dagger} c_{ia\sigma}, \quad (1)$$

* dawang@nju.edu.cn

† qhwang@nju.edu.cn

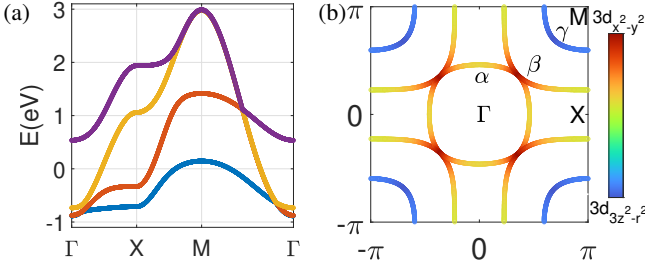


Figure 1. (a) Energy band dispersions along the high-symmetry path in the Brillouin zone. (b) Fermi surfaces with orbital components denoted by colors. The three pockets are labeled by α , β and γ , respectively.

where $c_{i\alpha\sigma}^\dagger$ creates an electron on site i with the orbital $a = x$ (for $3d_{x^2-y^2}$) or z (for $3d_{3z^2-r^2}$) and spin σ . The matrix element t_{δ}^{ab} is the hopping integral between a orbital on site i and b orbital on site $i + \delta$, and ϵ_a denotes the onsite energy of the a orbital. The tight-binding parameters are taken from Ref. [17]: $(t_{100}^{xx}, t_{110}^{xx}, t_{00\frac{1}{2}}^{xx}, t_{100}^{zz}, t_{110}^{zz}, t_{00\frac{1}{2}}^{zz}, t_{100}^{xz}, t_{10\frac{1}{2}}^{xz}, \epsilon_x, \epsilon_z) = (-0.483, 0.069, 0.005, -0.110, -0.017, -0.635, 0.239, -0.034, 0.776, 0.409)$ eV up to C_{4v} operations. Here, the distance between layers is assigned as $\frac{1}{2}$. The energy band dispersions and Fermi surfaces are shown in Fig. 1 with the orbital characters denoted by colors (red for $3d_{x^2-y^2}$ and blue for $3d_{3z^2-r^2}$). There are three Fermi pockets: α (electron-like pocket around Γ), β and γ (hole-like pockets around M). Note that the γ -pocket around M is mainly comprised of the $3d_{3z^2-r^2}$ orbital, suggesting considerable pairing component on the $3d_{3z^2-r^2}$ orbital, otherwise no pairing energy can be saved on the γ -pocket.

We consider the correlation effect by adding the onsite two-orbital Hubbard interactions given by

$$H_H = H_0 + \frac{1}{2} \sum_{i,a \neq b, \sigma \sigma'} (U' n_{ia\sigma} n_{ib\sigma'} + J_H c_{ia\sigma}^\dagger c_{ib\sigma} c_{ib\sigma'}^\dagger c_{ia\sigma'}) + \sum_{ia} U n_{ia\uparrow} n_{ia\downarrow} + \sum_{i,a \neq b} J_P c_{ia\uparrow}^\dagger c_{ia\downarrow}^\dagger c_{ib\downarrow} c_{ib\uparrow}, \quad (2)$$

where U/U' are intra/inter-orbital Coulomb repulsion, J_H is the Hund's coupling and J_P denotes the pair-hopping process. These four terms are assumed to satisfy the Kanamori relations [71]: $U = U' + 2J_H$ and $J_H = J_P$. Clearly, the bare Coulomb interactions are repulsive in the pairing channel and one needs to go beyond the bare interaction level to obtain superconductivity. For weak couplings, the spin/charge/pair fluctuations are captured by FRG on equal footing, which predicts the s_{\pm} -wave pairing [23]. The dominant pairing terms are shown in Fig. 2(a), including onsite pairing denoted by z_0/x_0 , pairing on the vertical bond z_1/x_1 , and pairing on the in-plane nearest neighbor bond z_2/x_2 . A typical gap function projected on the Fermi surfaces is shown in Fig. 2(c) with different signs on different pockets, hence, called s_{\pm} -wave pairing. As a comparison, for $d_{x^2-y^2}$ -wave pairing as the subleading instability in FRG, the real space pairing terms denoted by x_2/z_2 are sketched in Fig. 2(b) and the gap function on the

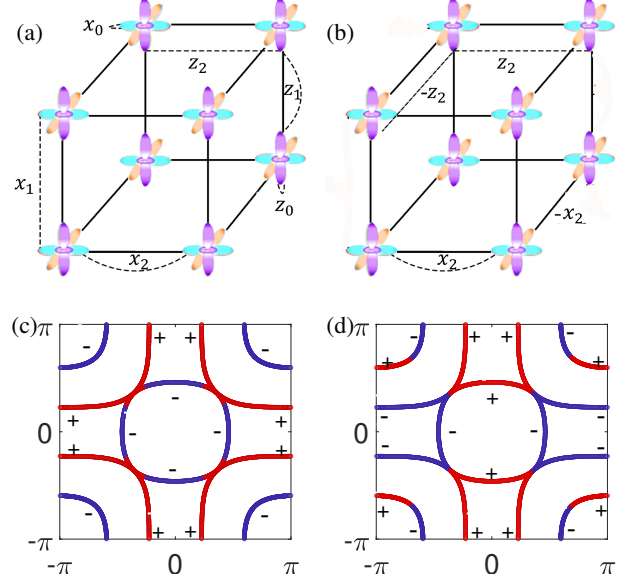


Figure 2. (a) Schematic plot of the pairing potentials (or variational pairing parameters in VQMC) for the s_{\pm} -wave pairing. Two orbitals, $3d_{3z^2-r^2}$ and $3d_{x^2-y^2}$, are assigned on each site. The dominant pairings between them are represented by $z_{0,1,2}$ and $x_{0,1,2}$, respectively. Here, 0 denotes onsite pairing, 1 denotes the vertical bond, 2 denotes the planar nearest neighbor bond. (b) is similar to (a) but for $d_{x^2-y^2}$ -wave pairing. In (c) and (d), the typical gap functions for the s_{\pm} -wave and $d_{x^2-y^2}$ -wave pairings are plotted on the Fermi surfaces with the sign indicated by colors (red for positive and blue for negative).

Fermi surfaces is plotted in Fig. 2(d).

On the other hand, in the strong coupling limit with $U \gtrsim U' \gg J_H$, the above Hubbard model can be mapped to a two-orbital $t - J$ model [23] in the subspace of one-electron (1e) and two-electrons (2e) per site since there are 1.5 electrons per site on average for $\text{La}_3\text{Ni}_2\text{O}_7$. The resulting $t - J$ Hamiltonian is

$$H_{tJ} = \sum_{\langle ij \rangle a, b, \sigma} \left(t_{ij}^{ab} c_{ia\sigma}^\dagger c_{jb\sigma} Q_{1e,i} Q_{2e,j} + \text{h.c.} \right) + \sum_{\langle ij \rangle a, n=1,2} J_{ij}^a \left(\mathbf{S}_{ia} \cdot \mathbf{S}_{ja} - \frac{1}{4} n_{ia} n_{ja} \right) Q_{ne,i} Q_{ne,j} + \sum_{i,a} J_H (Q_{2e,ia} - Q_{1e,ia} Q_{1e,i\bar{a}}) + \sum_{i,a>b} J_H \left(\frac{1}{4} n_{ia} n_{ib} - \mathbf{S}_{ia} \cdot \mathbf{S}_{ib} \right) Q_{1e,ia} Q_{1e,ib} + \sum_{i,a>b} J_P \left(c_{ia\uparrow}^\dagger c_{ia\downarrow}^\dagger c_{ib\downarrow} c_{ib\uparrow} + \text{h.c.} \right) + \sum_{ia} \frac{1}{2} (\epsilon_a - \epsilon_{\bar{a}}) (Q_{1e,ia} + 2Q_{2e,ia}), \quad (3)$$

where \bar{a} denotes the orbital other than a , \mathbf{S}_{ia} and n_{ia} are standard spin and charge operators for orbital a on site i , $Q_{ne,ia}$ is

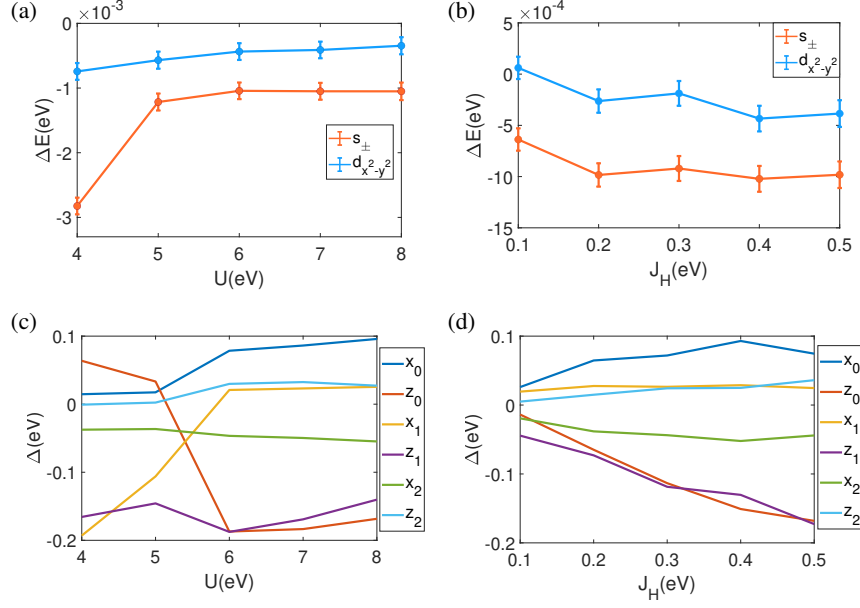


Figure 3. VQMC results of the $t-J$ model. The energies of the s_{\pm} -wave and $d_{x^2-y^2}$ -wave pairings relative to the normal state are plotted versus U by fixing $J_H = 0.5$ eV in (a), and versus J_H by fixing $U = 7$ eV in (b). The corresponding optimized variational pairing parameters for the s_{\pm} -wave are plotted versus U in (c) and versus J_H in (d), respectively.

the projection operator for n -electrons on orbital a and site i ,

$$\begin{aligned} Q_{0e,ia} &= (1 - n_{ia\uparrow})(1 - n_{ia\downarrow}), & Q_{2e,ia} &= n_{ia\uparrow}n_{ia\downarrow}, \\ Q_{1e,ia} &= n_{ia\uparrow}(1 - n_{ia\downarrow}) + (1 - n_{ia\uparrow})n_{ia\downarrow}, \end{aligned} \quad (4)$$

and $Q_{ne,i}$ is the projection operator for total charge n -electrons on site i ,

$$Q_{ne,i} = \sum_{k=0}^n Q_{ke,ix} Q_{(n-k)e,iz}. \quad (5)$$

The second line in Eq. 3 is the super-exchange (with $3e$ or $0e$ states as the intermediate states) $J_{ij}^a = 4(t_{ij}^{aa})^2/\bar{U}$ with $\bar{U} = (U + U')/2 = U - J_H$. The inter-orbital super-exchange is neglected due to small values of t_{ij}^{aa} and $t_{ij}^{aa}t_{ji}^{aa}$. Note that the above intra-orbital super-exchange term favors spin-singlet pairing at the mean field level, reminiscent of the single-orbital $t-J$ model for cuprates. Since the largest super-exchange is between the $3d_{3z^2-r^2}$ orbitals on the vertical bond, the s_{\pm} -pairing is expected to be favored with the dominant pairing component between the $3d_{3z^2-r^2}$ orbitals on this bond, as indicated by z_1 in Fig. 2(a). This is actually confirmed by previous RMFT calculations [23]. In the following, we further employ VQMC to investigate both the above $t-J$ and Hubbard models.

III. VQMC CALCULATIONS

In this section, we perform VQMC calculations to explore the superconducting properties of $\text{La}_3\text{Ni}_2\text{O}_7$. In VQMC, we take the ansatz that the superconducting ground state $|\Psi_G\rangle$ is

given by

$$|\Psi_G\rangle = \hat{P}|\Psi_0\rangle, \quad (6)$$

where \hat{P} is a suitable projection operator to be specified below and $|\Psi_0\rangle$ is the many body ground state of a free variational Hamiltonian defined as

$$H_v = \sum_{ijab\sigma} \left[h_{ij}^{ab} c_{ia\sigma}^\dagger c_{jb\sigma} + \sigma \left(\Delta_{ij}^a c_{ia\sigma}^\dagger c_{ja\bar{\sigma}}^\dagger + \text{H.c.} \right) \right], \quad (7)$$

where i and j denote lattice sites, a and b denote orbitals x/z , $\sigma = \pm 1$ denotes spin. The hopping integrals h_{ij}^{ab} (including onsite energies) and pairings Δ_{ij}^a are all variational parameters. In our calculations, we assume $h_{ij}^{ab} = g_{i,j}^{ab} t_{ij}^{ab}$. For pairing parameters Δ_{ij}^a , we consider the s_{\pm} -wave and $d_{x^2-y^2}$ -wave pairing ansatz, as shown in Fig. 2(a) and 2(b), respectively.

We specify the projection operator \hat{P} . For the $t-J$ model, we choose

$$\hat{P}_{tJ} = \prod_i (Q_{1e,i} + Q_{2e,i}) e^{-\sum_a g_a n_{ia\uparrow} n_{ia\downarrow}} e^{g_H m_{ix} m_{iz}}, \quad (8)$$

where $m_{ia} = (n_{ia\uparrow} - n_{ia\downarrow})$. The first term $(Q_{1e,i} + Q_{2e,i})$ is to project out the $1e$ and $2e$ subspace. In the second term, g_a is the Gutzwiller projection factor to suppress the double occupancy η_a for orbital a . In the third term, g_H is the Jastrow factor to promote the effect of the Hund's coupling.

Different from the $t-J$ model, the Hubbard model needs more careful treatment to obtain superconductivity, since the bare interactions do not favor superconductivity directly (in the mean field sense). Therefore, we need to add more Jastrow

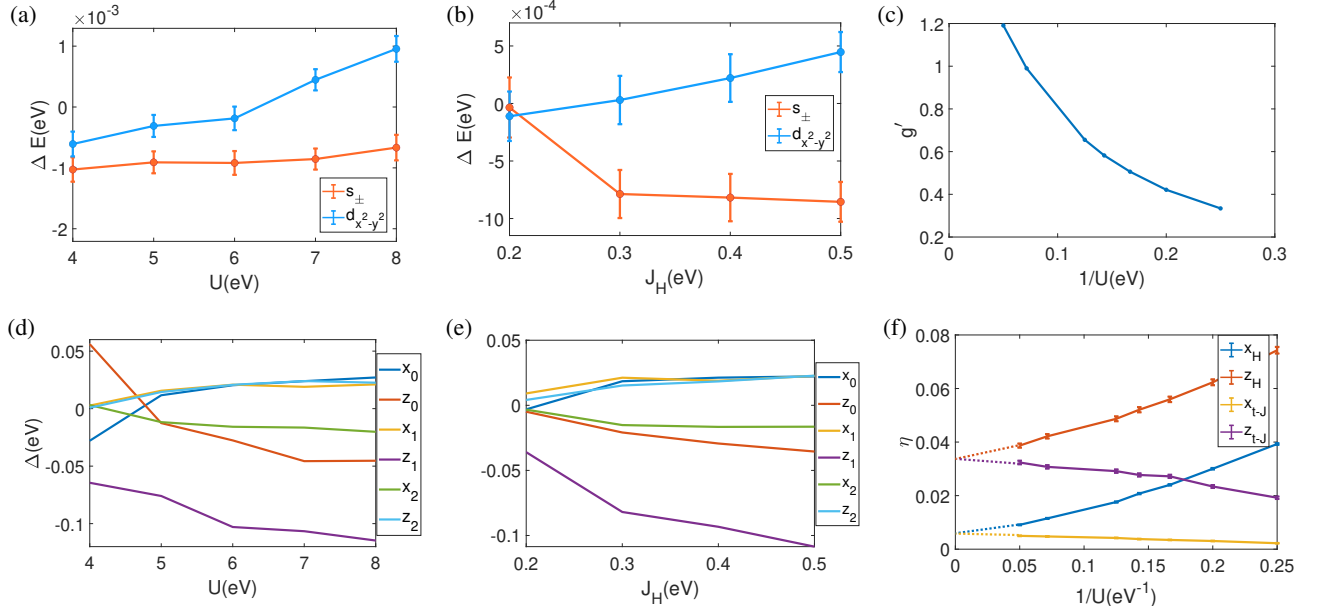


Figure 4. VQMC results of the Hubbard model. The energies of the s_{\pm} -wave and $d_{x^2-y^2}$ -wave pairings relative to the normal state are plotted versus U by fixing $J_H = 0.5$ eV in (a), and versus J_H by fixing $U = 7$ eV in (b). The Jastrow factor g' enforcing the $1e$ and $2e$ states (see Eq. 9) is plotted versus $1/U$ in (c). The optimized variational pairing parameters for the s_{\pm} -wave are plotted versus U in (d) and versus J_H in (e), respectively. In (f), the intra-orbital double occupancies η_x and η_z are plotted versus $1/U$ for both the $t-J$ (denoted by x_{t-J} and z_{t-J}) and Hubbard (denoted by x_H and z_H) models.

factors in the total projection operator giving

$$\hat{P}_H = \prod_i e^{g'_1(Q_{1e,i} + Q_{2e,i})} e^{-\sum_a g_a n_{ia}^\dagger n_{ia}} e^{g_H m_{ix} m_{iz}} \times \prod_{\langle ij \rangle} e^{g_1(Q_{0e,i} Q_{2e,j} + Q_{0e,j} Q_{2e,i})} e^{g_2(Q_{1e,i} Q_{3e,j} + Q_{1e,j} Q_{3e,i})}. \quad (9)$$

The first term g' is to promote the $1e$ and $2e$ states since all occupied states are allowed in the Hubbard model. The second and third terms are the same as the $t-J$ model. The last two Jastrow factors g_1 and g_2 are added to promote the doublon-holon processes involving $0e$ and $3e$ states, respectively, which are responsible for the super-exchange processes. In the above defined \hat{P}_{tJ} and \hat{P}_H , all the g factors are positive.

By VQMC, all the variational parameters h_{ij}^{ab} , Δ_{ij}^a , and the g -factors are optimized to minimize the total energy $\langle \psi_G | H_{H,tJ} | \psi_G \rangle$ for the Hubbard and $t-J$ models, respectively, using the stochastic reconfiguration technique. More technical details about the VQMC can be found in the appendix A. In practice, the periodic-antiperiodic boundary condition is adopt to avoid the open-shell problem. Most of our VQMC simulations are performed on the $L \times L \times 2$ lattice with $L = 6$, but larger sizes up to $L = 12$ have been checked, as shown in the appendix B, to ensure the finite size effect is acceptably small.

A. VQMC results of the $t-J$ model

We first present the results of the $t-J$ model. The optimized ground state energies of the s_{\pm} -wave and $d_{x^2-y^2}$ -wave pairings relative to the normal state are plotted versus U (by fixing $J_H = 0.5$ eV) in Fig. 3(a) and versus J_H (by fixing $U = 7$ eV) in Fig. 3(b), respectively. In the simulated parameter regime, the s_{\pm} -wave pairing always saves more energy than the $d_{x^2-y^2}$ -wave pairing, which is consistent with the early RMFT result [23] indicating the robustness of the s_{\pm} -wave pairing in $\text{La}_3\text{Ni}_2\text{O}_7$. With increasing U , the energy gain is found to be reduced, indicating the important role of the super-exchange $J = 4(t_{ij}^{aa})^2 / (U - J_H)$ in the superconducting mechanism in the large U limit, which is somewhat similar to the single-orbital $t-J$ model. On the other hand, the energy gain is also found to grow up with increasing J_H . These results indicate that both the super-exchange and the Hund's coupling promote the superconductivity in $\text{La}_3\text{Ni}_2\text{O}_7$ at least in the strong coupling (large U) limit.

We then examine the optimized pairing parameters for the s_{\pm} -wave pairing as shown in Fig. 3(c) versus U and in Fig. 3(d) versus J_H . Other variational parameters can be found in appendix B. Here, we focus on the pairing parameters. On-site pairing parameters Δ_{ii}^x (denoted by x_0) and Δ_{ii}^z (denoted by z_0) are anti-phase due to the pair-hopping interaction J_P . Note that the large x_0/z_0 does not necessarily lead to large order parameter $\langle c_{i,x/z,\downarrow} c_{i,x/z,\uparrow} \rangle$ because of the projection which suppresses the double occupancy (see below). Besides the on-site pairings, the dominant pairing is on the vertical bond Δ_{ij}^z

(denoted by z_1), which is much larger than $\Delta_{ij}^x(x_1)$, indicating the leading role of $3d_{3z^2-r^2}$ orbital in the s_{\pm} -wave pairing. As a comparison, the planar pairings z_2 and x_2 are relatively small. These results are also qualitatively consistent with the early RMFT calculations [23].

B. VQMC results of the Hubbard model

We turn to the more generic Hubbard model. As explained above, we need to add more Jastrow factors including g' (to enforce $1e$ and $2e$ states), g_1 and g_2 (to enforce doublon-holon process on the vertical and planar bonds). After VQMC optimization, our results are shown in Fig. 4. The energy gains of the s_{\pm} and $d_{x^2-y^2}$ pairings relative to the normal state are plotted versus U (fixing $J_H = 0.5$ eV) in Fig. 4(a) and versus J_H (fixing $U = 7$ eV) in Fig. 4(b). We find the s_{\pm} -wave pairing always saves more energy than the $d_{x^2-y^2}$ -wave pairing as long as $J_H > 0.2$ eV (very likely in $\text{La}_3\text{Ni}_2\text{O}_7$). This is one of the main results of the present work. It connects the weak- U limit (as studied by FRG) and strong- U limit ($t-J$ model as studied by RMFT), indicating the s_{\pm} -wave pairing is the most likely candidate of the pairing symmetry in $\text{La}_3\text{Ni}_2\text{O}_7$. Moreover, more energy gain is obtained for the s_{\pm} -wave pairing with decreasing U and/or increasing J_H , similar to the above $t-J$ model. This is consistent with the physical picture that both the super-exchange and Hund's coupling can promote the antiferromagnetic correlation on the vertical bond, which further induces the s_{\pm} -wave superconductivity.

Then we analyze the optimized variational parameters. In Fig. 4(c), the Jastrow factor g' (enforcing the $1e$ and $2e$ states) is found to grow up quickly as increasing U , confirming the validity of the $t-J$ model (living in the $1e$ and $2e$ subspace). In Fig. 4(d) and 4(e), we plot the optimized variational pairing parameters for the s_{\pm} -wave versus U and J_H , respectively. Other variational parameters and Jastrow factors can be found in appendix B. The leading pairing component is z_1 (between $3d_{3z^2-r^2}$ orbitals and on the vertical bond), which is consistent with the $t-J$ model and confirms the leading role of the $3d_{3z^2-r^2}$ orbital in the superconducting pairing. The subleading pairing components are z_0 and x_0 (onsite pairings) opposite signs, which is consistent with the atomic repulsive pair-hopping interaction.

Finally, we present the intra-orbital double occupancies $\eta_x = \langle Q_{2e,ix} \rangle$ and $\eta_z = \langle Q_{2e,iz} \rangle$ obtained in both the Hubbard and $t-J$ models, as shown in Fig. 4(f). For the Hubbard model, both η_x and η_z drops with increasing U , reflecting the effect of the Hubbard U on suppressing the double occupancy. Instead, for the $t-J$ model, both η_x and η_z grow up with increasing U rather than drops down. This seemingly paradox can be reconciled by the fact that the $t-J$ model already lives in the vicinity of $U = U' = \infty$ such that intra-orbital and inter-orbital double occupancies have no difference. We find in the limit of $U \rightarrow \infty$, both the Hubbard and $t-J$ models give the same double occupancies, which can be taken as a benchmark of the correctness of our VQMC simulations on both two models. Note that η_z keeps a finite value even as $U \rightarrow \infty$. This is quite different from the half-filled Hubbard

model, for which the local moment can be well defined by the vanishing of double occupancy. But for $\text{La}_3\text{Ni}_2\text{O}_7$, due to the non-integer filling fraction 1.5 per site, no well defined local moment exists even in the strong-coupling limit. This sheds light on the itinerant versus local moment picture of the electrons in this material.

IV. SUMMARY

In this work, we investigate the pairing symmetry in $\text{La}_3\text{Ni}_2\text{O}_7$ under pressure by applying VQMC on bilayer two-orbital $t-J$ and Hubbard models. We find the s_{\pm} -wave pairing is robust in most parameter regimes, which is consistent with the early FRG from weak to moderate correlation limit and RMFT for strong-coupling limit. The leading pairing component is found to be the one between $3d_{3z^2-r^2}$ orbitals on the vertical bond, indicating the important role of the $3d_{3z^2-r^2}$ orbital in superconducting $\text{La}_3\text{Ni}_2\text{O}_7$. We also find the intra-orbital double occupancies for the two orbitals remain finite even in the strong-coupling limit, shedding light on the itinerant versus local moment picture of the electrons in this material.

ACKNOWLEDGMENTS

This work is supported by National Key R&D Program of China (Grant No. 2022YFA1403201 and No. 2024YFA1408100) and National Natural Science Foundation of China (Grant No. 12374147, No. 12274205 and No. 92365203).

Appendix A: Details of VQMC method

We use \mathbf{X} to represent the set of variational parameters (x_1, x_2, \dots, x_μ) , and the variational free Hamiltonian can be written in a matrix form (in Nambu space) as

$$H_v = \phi^\dagger \mathbf{h}(\mathbf{X}) \phi, \quad (\text{A1})$$

where $\phi^\dagger = (c_{1\uparrow}^\dagger, c_{2\uparrow}^\dagger, \dots, c_{N\uparrow}^\dagger, c_{1\downarrow}, c_{2\downarrow}, \dots, c_{N\downarrow})$, $N = 4N'$ (two orbitals and two spins) with N' the number of unitcells, and $\mathbf{h}(\mathbf{X})$ is the Hamiltonian matrix in the basis of ϕ . In the following, we will not write out \mathbf{X} explicitly for simplicity. By diagonalization,

$$H_v = \phi^\dagger \mathbf{U} \mathbf{U}^\dagger \mathbf{h}(\mathbf{X}) \mathbf{U} \mathbf{U}^\dagger \phi = \psi^\dagger \mathbf{E} \psi = \sum_{\alpha} \lambda_{\alpha} \psi_{\alpha}^{\dagger} \psi_{\alpha}, \quad (\text{A2})$$

where the diagonal matrix $\mathbf{E} = \text{diag}(\lambda_1 \dots \lambda_{2N})$ contains $2N$ eigenvalues of \mathbf{h} , and \mathbf{U} is the unitary transformation matrix composed by eigenvectors $(\mu_{\alpha}, \nu_{\alpha})^t$ corresponding to λ_{α} . We suppose $\lambda_n \leq 0$ with $n \leq N$, and construct two $N \times N$ matrices

$$V_1 = (\mu_1, \mu_2 \dots \mu_N), \quad V_2 = (\nu_1, \nu_2 \dots \nu_N), \quad (\text{A3})$$

from which we can write down the ground state of H_v as

$$|\Psi_0\rangle = \left(\sum_{ij} c_{i\uparrow}^\dagger A_{ij} c_{j\downarrow}^\dagger \right)^{N_e/2} |0\rangle. \quad (\text{A4})$$

Here, $|0\rangle$ is the vacuum state, and $N_e = 3N/4$ is the total number of electrons, and

$$A = V_1 V_2^{-1}. \quad (\text{A5})$$

The ansatz of the variational ground state is

$$|\Psi_G\rangle = \hat{P}|\Psi_0\rangle, \quad (\text{A6})$$

where \hat{P} is a projection operator containing suitable Jastrow factors as specified in the main text. In the basis of real space many-body configuration $\{|R\rangle\}$, the variational ground state can be expanded as

$$|\Psi_G\rangle = \sum_R |R\rangle \langle R|\Psi_G\rangle = \sum_R f_R \det(A_R) |R\rangle, \quad (\text{A7})$$

where f_R is the projection factor for a given configuration $|R\rangle$, and $\det(A_R)$ is the determinant of the matrix A_R . The total energy of the Hubbard or $t - J$ model can be calculated as

$$\begin{aligned} E &= \frac{\langle \Psi_G | H | \Psi_G \rangle}{\langle \Psi_G | \Psi_G \rangle} \\ &= \frac{\sum_{RR'} f_R f_{R'} \det(A_R^*) \det(A_{R'}) \langle R | H | R' \rangle}{\sum_R f_R^2 |\det(A_R)|^2} \\ &= \frac{\sum_R f_R^2 |\det(A_R)|^2 \sum_{R'} \frac{f_{R'}}{f_R} \frac{\det(A_{R'})}{\det(A_R)} \langle R | H | R' \rangle}{\sum_R f_R^2 |\det(A_R)|^2} \\ &= \left\langle \sum_{R'} \frac{f_{R'}}{f_R} \frac{\det(A_{R'})}{\det(A_R)} \langle R | H | R' \rangle \right\rangle, \end{aligned} \quad (\text{A8})$$

where we have defined the Monte Carlo average $\langle \dots \rangle$ with the configuration weight $w_R = f_R^2 |\det(A_R)|^2$, i.e.

$$\langle \dots \rangle = \frac{\sum_R (\dots) w_R}{\sum_R w_R}. \quad (\text{A9})$$

Next, to optimize the variational parameters \mathbf{X} , we adopt the stochastic reconfiguration method [72, 73] to update x_μ . In the usual gradient descent method,

$$dx_\mu = -\frac{\partial E}{\partial x_\mu} dt, \quad (\text{A10})$$

where dt is an artificial time step. After updating all variational parameters, we have

$$|\Psi_G\rangle \rightarrow |\Psi_G\rangle + \sum_\mu dx_\mu |\mu\rangle, \quad (\text{A11})$$

where $|\mu\rangle \equiv \partial |\Psi_G\rangle / \partial x_\mu$. However, this updating strategy is not always stable since the states $|\mu\rangle$ are not be orthogonal to each other in general such that the variational parameters are not independent and the update in x_μ could have a huge influence on x_ν . As a remedy, we can choose a set of orthogonal basis $\{|a\rangle\}$ such that

$$dx_a = -\frac{\partial E}{\partial x_a} dt. \quad (\text{A12})$$

and

$$\sum_a dx_a |a\rangle = \sum_\mu dx_\mu |\mu\rangle. \quad (\text{A13})$$

Left-multiplying with $\langle \nu |$ on the two sides, we have

$$\sum_a dx_a \langle \nu | a \rangle = \sum_\mu \langle \nu | \mu \rangle dx_\mu \equiv \sum_\mu g_{\nu\mu} dx_\mu, \quad (\text{A14})$$

where we have defined $g_{\nu\mu} \equiv \langle \nu | \mu \rangle$. Then, left-multiplying with $(g^{-1})_{\mu'\nu}$, summing over a, μ, ν , and then replacing μ' with μ , we obtain the revised update equation

$$dx_\mu = -\sum_\nu (g^{-1})_{\mu\nu} \frac{\partial E}{\partial x_\nu} dt. \quad (\text{A15})$$

In general, the matrix g could have eigenvalues approaching zero, which could cause instability when calculating the inverse of g . We can add a small positive number ε to the diagonal elements of g , i.e., $g_{\mu\mu} \rightarrow (1 + \varepsilon)g_{\mu\mu}$. Now we can update x_μ as long as we obtain the matrix $g_{\mu\nu}$ and $\partial_\nu E$, which can be calculated in the basis of $|R\rangle$ as

$$g_{\mu\nu} = \langle l_\mu^* | l_\nu \rangle - \text{Re} \langle l_\mu \rangle \text{Re} \langle l_\nu \rangle + i[\text{Im} \langle l_\mu \rangle \text{Re} \langle l_\nu \rangle - (\mu \leftrightarrow \nu)], \quad (\text{A16})$$

$$\partial_\nu E = \langle h | l_\nu \rangle - E \langle l_\nu \rangle + c.c., \quad (\text{A17})$$

where

$$\begin{aligned} l_\mu(R) &\equiv \partial_\mu \ln[f_R \det(A_R)] \\ &= \text{Tr}(A_R^{-1} \partial_\mu A_R) + \partial_\mu \ln(f_R). \end{aligned} \quad (\text{A18})$$

Appendix B: More VQMC results

In this section, we supplement more results of our VQMC simulations. In Fig. 5, we plot the energies of the s_\pm -wave and $d_{x^2-y^2}$ -wave pairings for the $t - J$ model on different lattice size L (from 6 to 12) to examine the finite size effect. We find the energies does not change with L significantly, in particular the relative energies between the two pairing candidates.

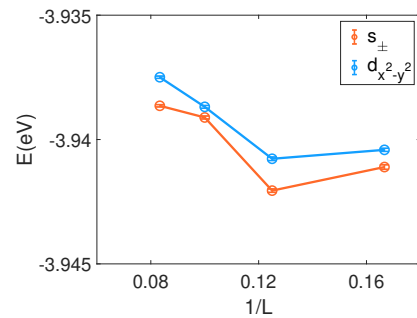


Figure 5. Finite size effect with lattice size $L = 6$ to 12 for the energies of the s_\pm -wave and $d_{x^2-y^2}$ -wave pairings at $U = 7$ eV and $J_H = 0.5$ eV.

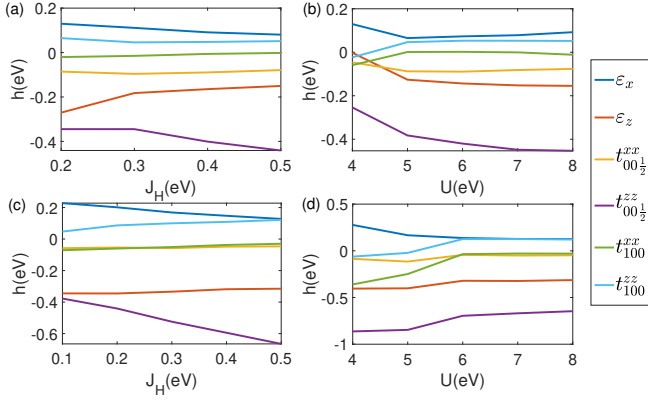


Figure 6. The optimized variational hopping and onsite energy parameters for the Hubbard model are plotted versus J_H at $U = 7$ eV in (a), and versus U at $J_H = 0.5$ eV in (b). (c,d) are similar to (a,b) but for the $t - J$ model.

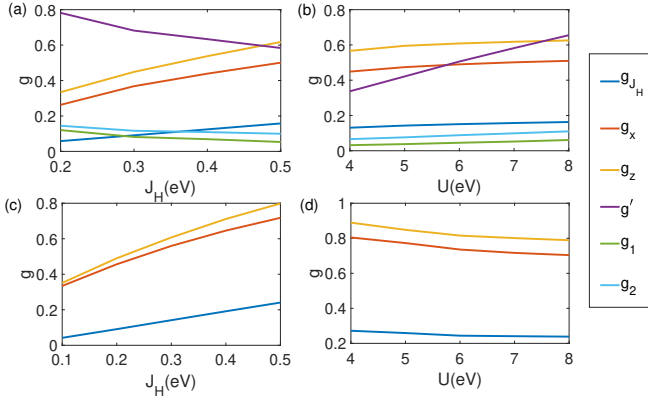


Figure 7. The optimized Jastrow factors for the Hubbard model are plotted versus J_H at $U = 7$ eV in (a), and versus U at $J_H = 0.5$ eV in (b). (c,d) are similar to (a,b) but for the $t - J$ model.

This indicates that $L = 6$ is large enough and reliable to identify the pairing symmetry. We next present more optimized variational hoppings and onsite energies in the free variational Hamiltonian H_V relative to the bare values in the tight-binding Hamiltonian H_0 . The inter-layer hopping between the $3d_{3z^2-r^2}$ orbitals $h_{00\frac{1}{2}}^{zz}$ keeps to have the largest amplitude, indicating its important role (e.g. for super-exchange) even in the strong-coupling limit. In Fig. 7, we present the optimized Jastrow factors. In particular, $g_{x,z}$ (to suppress intra-orbital double occupancy) grows up with increasing U , consistent with the double occupancies $\eta_{x,z}$ as shown in the main text.

-
- [1] H. Sun, M. Huo, X. Hu, J. Li, Z. Liu, Y. Han, L. Tang, Z. Mao, P. Yang, B. Wang, J. Cheng, D.-X. Yao, G.-M. Zhang, and M. Wang, Signatures of superconductivity near 80 K in a nickelate under high pressure, *Nature* **621**, 493 (2023).
 - [2] Y. Zhang, D. Su, Y. Huang, Z. Shan, H. Sun, M. Huo, K. Ye, J. Zhang, Z. Yang, Y. Xu, Y. Su, R. Li, M. Smidman, M. Wang, L. Jiao, and H. Yuan, High-temperature superconductivity with zero resistance and strange-metal behaviour in $\text{La}_3\text{Ni}_2\text{O}_{7-\delta}$, *Nature Physics* **20**, 1269 (2024).
 - [3] J. Hou, P.-T. Yang, Z.-Y. Liu, J.-Y. Li, P.-F. Shan, L. Ma, G. Wang, N.-N. Wang, H.-Z. Guo, J.-P. Sun, Y. Uwatoko, M. Wang, G.-M. Zhang, B.-S. Wang, and J.-G. Cheng, Emergence of high-temperature superconducting phase in pressurized $\text{La}_3\text{Ni}_2\text{O}_7$ crystals, *Chinese Physics Letters* **40**, 117302 (2023).
 - [4] Z. Liu, M. Huo, J. Li, Q. Li, Y. Liu, Y. Dai, X. Zhou, J. Hao, Y. Lu, M. Wang, and H.-H. Wen, Electronic correlations and partial gap in the bilayer nickelate $\text{La}_3\text{Ni}_2\text{O}_7$, *Nature Communications* **15**, 7570 (2024).
 - [5] G. Wang, N. N. Wang, X. L. Shen, J. Hou, L. Ma, L. F. Shi, Z. A. Ren, Y. D. Gu, H. M. Ma, P. T. Yang, Z. Y. Liu, H. Z. Guo, J. P. Sun, G. M. Zhang, S. Calder, J.-Q. Yan, B. S. Wang, Y. Uwatoko, and J.-G. Cheng, Pressure-induced superconductivity in polycrystalline $\text{La}_3\text{Ni}_2\text{O}_{7-\delta}$, *Phys. Rev. X* **14**, 011040 (2024).
 - [6] L. C. Rhodes and P. Wahl, Structural routes to stabilize superconducting $\text{La}_3\text{Ni}_2\text{O}_7$ at ambient pressure, *Phys. Rev. Mater.* **8**, 044801 (2024).
 - [7] J. Yang, H. Sun, X. Hu, Y. Xie, T. Miao, H. Luo, H. Chen, B. Liang, W. Zhu, G. Qu, C.-Q. Chen, M. Huo, Y. Huang, S. Zhang, F. Zhang, F. Yang, Z. Wang, Q. Peng, H. Mao, G. Liu, Z. Xu, T. Qian, D.-X. Yao, M. Wang, L. Zhao, and X. J. Zhou, Orbital-dependent electron correlation in double-layer nickelate $\text{La}_3\text{Ni}_2\text{O}_7$, *Nature Communications* **15**, 4373 (2024).
 - [8] Y. Zhou, J. Guo, S. Cai, H. Sun, C. Li, J. Zhao, P. Wang, J. Han, X. Chen, Y. Chen, Q. Wu, Y. Ding,

- T. Xiang, H.-k. Mao, and L. Sun, Investigations of key issues on the reproducibility of high- T_c superconductivity emerging from compressed $\text{La}_3\text{Ni}_2\text{O}_7$, *Matter and Radiation at Extremes* **10**, 027801 (2025).
- [9] L. Wang, Y. Li, S.-Y. Xie, F. Liu, H. Sun, C. Huang, Y. Gao, T. Nakagawa, B. Fu, B. Dong, Z. Cao, R. Yu, S. I. Kawaguchi, H. Kadobayashi, M. Wang, C. Jin, H.-k. Mao, and H. Liu, Structure responsible for the superconducting state in $\text{La}_3\text{Ni}_2\text{O}_7$ at high-pressure and low-temperature conditions, *Journal of the American Chemical Society* **146**, 7506 (2024).
- [10] M. Kakoi, T. Oi, Y. Ohshita, M. Yashima, K. Kuroki, T. Kato, H. Takahashi, S. Ishiwata, Y. Adachi, N. Hatada, T. Uda, and H. Mukuda, Multiband metallic ground state in multilayered nickelates $\text{La}_3\text{Ni}_2\text{O}_7$ and $\text{La}_4\text{Ni}_3\text{O}_{10}$ probed by ^{139}La -NMR at ambient pressure, *Journal of the Physical Society of Japan* **93**, 053702 (2024).
- [11] H. Wang, L. Chen, A. Rutherford, H. Zhou, and W. Xie, Long-range structural order in a hidden phase of ruddlesden–popper bilayer nickelate $\text{La}_3\text{Ni}_2\text{O}_7$, *Inorganic Chemistry* **63**, 5020 (2024).
- [12] X. Chen, J. Zhang, A. S. Thind, S. Sharma, H. LaBollita, G. Peterson, H. Zheng, D. P. Phelan, A. S. Botana, R. F. Klie, and J. F. Mitchell, Polymorphism in the ruddlesden–popper nickelate $\text{La}_3\text{Ni}_2\text{O}_7$: Discovery of a hidden phase with distinctive layer stacking, *Journal of the American Chemical Society* **10.1021/jacs.3c14052** (2024).
- [13] D. Zhao, Y. Zhou, M. Huo, Y. Wang, L. Nie, Y. Yang, J. Ying, M. Wang, T. Wu, and X. Chen, Pressure-enhanced spin-density-wave transition in double-layer nickelate $\text{La}_3\text{Ni}_2\text{O}_{7-\delta}$, *Science Bulletin* **70**, 1239 (2025).
- [14] X. Chen, J. Choi, Z. Jiang, J. Mei, K. Jiang, J. Li, S. Agrestini, M. Garcia-Fernandez, H. Sun, X. Huang, D. Shen, M. Wang, J. Hu, Y. Lu, K.-J. Zhou, and D. Feng, Electronic and magnetic excitations in $\text{La}_3\text{Ni}_2\text{O}_7$, *Nature Communications* **15**, 9597 (2024).
- [15] B. Geisler, L. Fanfarillo, J. J. Hamlin, G. R. Stewart, R. G. Hennig, and P. J. Hirschfeld, Optical properties and electronic correlations in $\text{La}_3\text{Ni}_2\text{O}_7$ bilayer nickelates under high pressure, *npj Quantum Materials* **9**, 89 (2024).
- [16] J. Zhan, Y. Gu, X. Wu, and J. Hu, Cooperation between electron-phonon coupling and electronic interaction in bilayer nickelates $\text{La}_3\text{Ni}_2\text{O}_7$, *Phys. Rev. Lett.* **134**, 136002 (2025).
- [17] Z. Luo, X. Hu, M. Wang, W. Wú, and D.-X. Yao, Bilayer two-orbital model of $\text{La}_3\text{Ni}_2\text{O}_7$ under pressure, *Phys. Rev. Lett.* **131**, 126001 (2023).
- [18] D. A. Shilenko and I. V. Leonov, Correlated electronic structure, orbital-selective behavior, and magnetic correlations in double-layer $\text{La}_3\text{Ni}_2\text{O}_7$ under pressure, *Phys. Rev. B* **108**, 125105 (2023).
- [19] Y. Shen, M. Qin, and G.-M. Zhang, Effective bi-layer model hamiltonian and density-matrix renormalization group study for the high- T_c superconductivity in $\text{La}_3\text{Ni}_2\text{O}_7$ under high pressure, *Chinese Physics Letters* **40**, 127401 (2023).
- [20] F. Lechermann, J. Gondolf, S. Bötzel, and I. M. Eremin, Electronic correlations and superconducting instability in $\text{La}_3\text{Ni}_2\text{O}_7$ under high pressure, *Phys. Rev. B* **108**, L201121 (2023).
- [21] Y. Gu, C. Le, Z. Yang, X. Wu, and J. Hu, Effective model and pairing tendency in the bilayer ni-based superconductor $\text{La}_3\text{Ni}_2\text{O}_7$, *Phys. Rev. B* **111**, 174506 (2025).
- [22] H. Sakakibara, N. Kitamine, M. Ochi, and K. Kuroki, Possible high T_c superconductivity in $\text{La}_3\text{Ni}_2\text{O}_7$ under high pressure through manifestation of a nearly half-filled bilayer hubbard model, *Phys. Rev. Lett.* **132**, 106002 (2024).
- [23] Q.-G. Yang, D. Wang, and Q.-H. Wang, Possible s_{\pm} -wave superconductivity in $\text{La}_3\text{Ni}_2\text{O}_7$, *Phys. Rev. B* **108**, L140505 (2023).
- [24] Y. Zhang, L.-F. Lin, A. Moreo, and E. Dagotto, Electronic structure, dimer physics, orbital-selective behavior, and magnetic tendencies in the bilayer nickelate superconductor $\text{La}_3\text{Ni}_2\text{O}_7$ under pressure, *Phys. Rev. B* **108**, L180510 (2023).
- [25] X.-Z. Qu, D.-W. Qu, J. Chen, C. Wu, F. Yang, W. Li, and G. Su, Bilayer $t-J-J_{\perp}$ model and magnetically mediated pairing in the pressurized nickelate $\text{La}_3\text{Ni}_2\text{O}_7$, *Phys. Rev. Lett.* **132**, 036502 (2024).
- [26] H. Oh and Y.-H. Zhang, Type-II $t-J$ model and shared superexchange coupling from hund’s rule in superconducting $\text{La}_3\text{Ni}_2\text{O}_7$, *Phys. Rev. B* **108**, 174511 (2023).
- [27] W. Wú, Z. Luo, D.-X. Yao, and M. Wang, Superexchange and charge transfer in the nickelate superconductor $\text{La}_3\text{Ni}_2\text{O}_7$ under pressure, *Science China Physics, Mechanics & Astronomy* **67**, 117402 (2024).
- [28] Z. Liao, L. Chen, G. Duan, Y. Wang, C. Liu, R. Yu, and Q. Si, Electron correlations and superconductivity in $\text{La}_3\text{Ni}_2\text{O}_7$ under pressure tuning, *Phys. Rev. B* **108**, 214522 (2023).
- [29] Y. Zhang, L.-F. Lin, A. Moreo, T. A. Maier, and E. Dagotto, Structural phase transition, s_{\pm} -wave pairing, and magnetic stripe order in bilayered superconductor $\text{La}_3\text{Ni}_2\text{O}_7$ under pressure, *Nature Communications* **15**, 2470 (2024).
- [30] C. Lu, Z. Pan, F. Yang, and C. Wu, Interlayer-coupling-driven high-temperature superconductivity in $\text{La}_3\text{Ni}_2\text{O}_7$ under pressure, *Phys. Rev. Lett.* **132**, 146002 (2024).
- [31] Y.-B. Liu, J.-W. Mei, F. Ye, W.-Q. Chen, and F. Yang, s_{\pm} -wave pairing and the destructive role of apical-oxygen deficiencies in $\text{La}_3\text{Ni}_2\text{O}_7$ under pressure, *Phys. Rev. Lett.* **131**, 236002 (2023).
- [32] X. Chen, P. Jiang, J. Li, Z. Zhong, and Y. Lu, Charge and spin instabilities in superconducting $\text{La}_3\text{Ni}_2\text{O}_7$, *Phys. Rev. B* **111**, 014515 (2025).
- [33] Y. Cao and Y.-f. Yang, Flat bands promoted by hund’s rule coupling in the candidate double-layer high-temperature superconductor $\text{La}_3\text{Ni}_2\text{O}_7$ under high pressure, *Phys. Rev. B* **109**, L081105 (2024).
- [34] V. Christiansson, F. Petocchi, and P. Werner, Correlated electronic structure of $\text{La}_3\text{Ni}_2\text{O}_7$ under pressure, *Phys. Rev. Lett.* **131**, 206501 (2023).
- [35] Z. Luo, B. Lv, M. Wang, W. Wú, and D.-X. Yao, High- T_c superconductivity in $\text{La}_3\text{Ni}_2\text{O}_7$ based on the bilayer two-orbital t-j model, *npj Quantum Materials* **9**, 61 (2024).
- [36] R. Jiang, J. Hou, Z. Fan, Z.-J. Lang, and W. Ku, Pressure driven fractionalization of ionic spins results in cupratelike high- T_c superconductivity in $\text{La}_3\text{Ni}_2\text{O}_7$, *Phys. Rev. Lett.* **132**, 126503 (2024).
- [37] Y.-H. Tian, Y. Chen, J.-M. Wang, R.-Q. He, and Z.-Y. Lu, Correlation effects and concomitant two-orbital s_{\pm} -wave superconductivity in $\text{La}_3\text{Ni}_2\text{O}_7$ under high pressure, *Phys. Rev. B* **109**, 165154 (2024).
- [38] Q. Qin and Y.-f. Yang, High- T_c superconductivity by mobilizing local spin singlets and possible route to higher T_c in pressurized $\text{La}_3\text{Ni}_2\text{O}_7$, *Phys. Rev. B* **108**, L140504 (2023).
- [39] J. Huang, Z. D. Wang, and T. Zhou, Impurity and vortex states in the bilayer high-temperature superconductor $\text{La}_3\text{Ni}_2\text{O}_7$, *Phys. Rev. B* **108**, 174501 (2023).
- [40] K. Jiang, Z. Wang, and F.-C. Zhang, High-temperature superconductivity in $\text{La}_3\text{Ni}_2\text{O}_7$, *Chinese Physics Letters* **41**, 017402 (2024).
- [41] Y.-f. Yang, G.-M. Zhang, and F.-C. Zhang, Interlayer valence bonds and two-component theory for high-

- T_c superconductivity of $\text{La}_3\text{Ni}_2\text{O}_7$ under pressure, *Phys. Rev. B* **108**, L201108 (2023).
- [42] H. Lange, L. Homeier, E. Demler, U. Schollwöck, F. Grusdt, and A. Bohrdt, Feshbach resonance in a strongly repulsive ladder of mixed dimensionality: A possible scenario for bilayer nickelate superconductors, *Phys. Rev. B* **109**, 045127 (2024).
- [43] H. Yang, H. Oh, and Y.-H. Zhang, Strong pairing from a small fermi surface beyond weak coupling: Application to $\text{La}_3\text{Ni}_2\text{O}_7$, *Phys. Rev. B* **110**, 104517 (2024).
- [44] S. Ryee, N. Witt, and T. O. Wehling, Quenched pair breaking by interlayer correlations as a key to superconductivity in $\text{La}_3\text{Ni}_2\text{O}_7$, *Phys. Rev. Lett.* **133**, 096002 (2024).
- [45] C. Lu, Z. Pan, F. Yang, and C. Wu, Interplay of two E_g orbitals in superconducting $\text{La}_3\text{Ni}_2\text{O}_7$ under pressure, *Phys. Rev. B* **110**, 094509 (2024).
- [46] T. Kaneko, H. Sakakibara, M. Ochi, and K. Kuroki, Pair correlations in the two-orbital hubbard ladder: Implications for superconductivity in the bilayer nickelate $\text{La}_3\text{Ni}_2\text{O}_7$, *Phys. Rev. B* **109**, 045154 (2024).
- [47] R. Gao, L. Jin, S. Huyan, D. Ni, H. Wang, X. Xu, S. L. Bud'ko, P. Canfield, W. Xie, and R. J. Cava, Is $\text{La}_3\text{Ni}_2\text{O}_{6.5}$ a bulk superconducting nickelate?, *ACS Applied Materials & Interfaces* **16**, 66857 (2024).
- [48] Z. Ouyang, J.-M. Wang, J.-X. Wang, R.-Q. He, L. Huang, and Z.-Y. Lu, Hund electronic correlation in $\text{La}_3\text{Ni}_2\text{O}_7$ under high pressure, *Phys. Rev. B* **109**, 115114 (2024).
- [49] J. Chen, F. Yang, and W. Li, Orbital-selective superconductivity in the pressurized bilayer nickelate $\text{La}_3\text{Ni}_2\text{O}_7$: An infinite projected entangled-pair state study, *Phys. Rev. B* **110**, L041111 (2024).
- [50] K. Chen, X. Liu, J. Jiao, M. Zou, C. Jiang, X. Li, Y. Luo, Q. Wu, N. Zhang, Y. Guo, and L. Shu, Evidence of spin density waves in $\text{La}_3\text{Ni}_2\text{O}_{7-\delta}$, *Phys. Rev. Lett.* **132**, 256503 (2024).
- [51] H. Schlömer, U. Schollwöck, F. Grusdt, and A. Bohrdt, Superconductivity in the pressurized nickelate $\text{La}_3\text{Ni}_2\text{O}_7$ in the vicinity of a BEC-BCS crossover, *Communications Physics* **7**, 366 (2024).
- [52] Y.-Y. Zheng and W. Wú, s_{\pm} -wave superconductivity in the bilayer two-orbital hubbard model, *Phys. Rev. B* **111**, 035108 (2025).
- [53] Z. Dong, M. Huo, J. Li, J. Li, P. Li, H. Sun, L. Gu, Y. Lu, M. Wang, Y. Wang, and Z. Chen, Visualization of oxygen vacancies and self-doped ligand holes in $\text{La}_3\text{Ni}_2\text{O}_{7-\delta}$, *Nature* **630**, 847 (2024).
- [54] G. Heier, K. Park, and S. Y. Savrasov, Competing d_{xy} and s_{\pm} pairing symmetries in superconducting $\text{La}_3\text{Ni}_2\text{O}_7$: LDA + FLEX calculations, *Phys. Rev. B* **109**, 104508 (2024).
- [55] M. Kakoi, T. Kaneko, H. Sakakibara, M. Ochi, and K. Kuroki, Pair correlations of the hybridized orbitals in a ladder model for the bilayer nickelate $\text{La}_3\text{Ni}_2\text{O}_7$, *Phys. Rev. B* **109**, L201124 (2024).
- [56] Y. Wang, K. Jiang, Z. Wang, F.-C. Zhang, and J. Hu, Electronic and magnetic structures of bilayer $\text{La}_3\text{Ni}_2\text{O}_7$ at ambient pressure, *Phys. Rev. B* **110**, 205122 (2024).
- [57] S. Bötzel, F. Lechermann, J. Gondolf, and I. M. Eremin, Theory of magnetic excitations in the multilayer nickelate superconductor $\text{La}_3\text{Ni}_2\text{O}_7$, *Phys. Rev. B* **109**, L180502 (2024).
- [58] X.-W. Yi, Y. Meng, J.-W. Li, Z.-W. Liao, W. Li, J.-Y. You, B. Gu, and G. Su, Nature of charge density waves and metal-insulator transition in pressurized $\text{La}_3\text{Ni}_2\text{O}_7$, *Phys. Rev. B* **110**, L140508 (2024).
- [59] Z. Ouyang, M. Gao, and Z.-Y. Lu, Absence of electron-phonon coupling superconductivity in the bilayer phase of $\text{La}_3\text{Ni}_2\text{O}_7$ under pressure, *npj Quantum Materials* **9**, 80 (2024).
- [60] H. Oh, B. Zhou, and Y.-H. Zhang, Type-II t - J model in charge transfer regime in bilayer $\text{La}_3\text{Ni}_2\text{O}_7$ and trilayer $\text{La}_4\text{Ni}_3\text{O}_{10}$, *Phys. Rev. B* **111**, L020504 (2025).
- [61] D. Li, K. Lee, B. Y. Wang, M. Osada, S. Crossley, H. R. Lee, Y. Cui, Y. Hikita, and H. Y. Hwang, Superconductivity in an infinite-layer nickelate, *Nature* **572**, 624 (2019).
- [62] Z. Pan, C. Lu, F. Yang, and C. Wu, Effect of rare-earth element substitution in superconducting $\text{R}_3\text{Ni}_2\text{O}_7$ under pressure, *Chinese Physics Letters* **41**, 087401 (2024).
- [63] Y. Zhang, L.-F. Lin, A. Moreo, T. A. Maier, and E. Dagotto, Trends in electronic structures and s_{\pm} -wave pairing for the rare-earth series in bilayer nickelate superconductor $\text{R}_3\text{Ni}_2\text{O}_7$, *Phys. Rev. B* **108**, 165141 (2023).
- [64] H. Sakakibara, M. Ochi, H. Nagata, Y. Ueki, H. Sakurai, R. Matsumoto, K. Terashima, K. Hirose, H. Ohta, M. Kato, Y. Takano, and K. Kuroki, Theoretical analysis on the possibility of superconductivity in the trilayer ruddlesden-popper nickelate $\text{La}_4\text{Ni}_3\text{O}_{10}$ under pressure and its experimental examination: Comparison with $\text{La}_3\text{Ni}_2\text{O}_7$, *Phys. Rev. B* **109**, 144511 (2024).
- [65] M. Zhang, C. Pei, D. Peng, X. Du, W. Hu, Y. Cao, Q. Wang, J. Wu, Y. Li, H. Liu, C. Wen, J. Song, Y. Zhao, C. Li, W. Cao, S. Zhu, Q. Zhang, N. Yu, P. Cheng, L. Zhang, Z. Li, J. Zhao, Y. Chen, C. Jin, H. Guo, C. Wu, F. Yang, Q. Zeng, S. Yan, L. Yang, and Y. Qi, Superconductivity in trilayer nickelate $\text{La}_4\text{Ni}_3\text{O}_{10}$ under pressure, *Phys. Rev. X* **15**, 021005 (2025).
- [66] A. A. Carrasco Álvarez, S. Petit, L. Iglesias, M. Bibes, W. Prellier, and J. Varignon, Electron-phonon mediated superconductivity in $\text{La}_6\text{Ni}_5\text{O}_{12}$ nickel oxides, *Phys. Rev. B* **110**, 235107 (2024).
- [67] J. G. Bednorz and K. A. Müller, Possible high T_c superconductivity in the Ba-La-Cu-O system, *Zeitschrift für Physik B Condensed Matter* **64**, 189 (1986).
- [68] M. U. Ubbens and P. A. Lee, Spin-gap formation in bilayer cuprates due to enhanced interlayer pairing, *Phys. Rev. B* **50**, 438 (1994).
- [69] J. Maly, D. Z. Liu, and K. Levin, Superconducting order parameter symmetry in multilayer cuprates, *Phys. Rev. B* **53**, 6786 (1996).
- [70] R. Eder, Y. Ohta, and S. Maekawa, Ground-state properties and dynamics of the bilayer t - J model, *Phys. Rev. B* **52**, 7708 (1995).
- [71] C. Castellani, C. R. Natoli, and J. Ranninger, Magnetic structure of V_2O_3 in the insulating phase, *Phys. Rev. B* **18**, 4945 (1978).
- [72] S. Sorella, Wave function optimization in the variational monte carlo method, *Phys. Rev. B* **71**, 241103 (2005).
- [73] J. Toulouse and C. Umrigar, Optimization of quantum monte carlo wave functions by energy minimization, *The Journal of chemical physics* **126**, 084102 (2007).